Journal of Atmospheric and Solar-Terrestrial Physics 86 (2012) 71–82

Contents lists available at SciVerse ScienceDirect

Journal of Atmospheric and Solar-Terrestrial Physics

journal homepage: www.elsevier.com/locate/jastp

Atmospheric delay analysis from GPS meteorology and InSAR APS

Shilai Cheng [a,b], Daniele Perissin [a,*,1], Hui Lin [a], Fulong Chen [a]

[a] Institute of Space and Earth Information Science, Chinese University of Hong Kong, Hong Kong
[b] GNSS Research Center, Wuhan University, China

ARTICLE INFO

Article history:
Received 6 April 2011
Received in revised form
2 June 2012
Accepted 10 June 2012
Available online 19 June 2012

Keywords:
SAR interferometry
GPS
Atmospheric phase screen
Zenith tropospheric delay

ABSTRACT

Radar atmospheric decorrelation due to inhomogeneity of atmospheric refractivity is a critical limitation of satellite SAR interferometry (InSAR) in the high accuracy retrieving of geophysical parameters. With mm precision, a water vapor tracing technique based on GPS meteorology was widely employed to mitigate InSAR atmospheric errors. However, a reliable comparison of atmospheric delay between GPS and InSAR is rarely touched, mainly due to the scarcity of stable and accurate InSAR atmospheric phases. In the paper we propose a comparison methodology between GPS Zenith Tropospheric Delay (ZTD) and SAR Atmospheric Phase Screen (APS) in both differential and pseudo-absolute modes. In the experiment, ENVISAT ASAR APS maps and synchronous GPS campaign measurements in Como, Italy were collected for consistency analysis. Furthermore, the stratification effect of atmospheric delay, in a form of delay-to-elevation ratios, was particularly analyzed for the purpose of separating different components within APSs. Finally, with the above stratification analysis, terms of stratification and assumed turbulence from SAR APS and GPS were compared in differential mode. Presented results show that the stratified ratios from GPS delays and SAR APS maps are in agreement with a std of 7.7 mm/km and a bias of 3.4 mm/km. Correlation coefficients of stratified ratios are higher than 0.7 in ascending case. In differential mode, the atmospheric total delays coincide with STandard Deviations (STDs) smaller than 4 mm (~0.65 mm PWV) and with correlation coefficients higher than 0.6. The comparison of total delays in 'pseudo-absolute' mode is provided as an alternative vision of the agreement between GPS and InSAR. The agreement in this mode was slightly worse than that in differential mode. STDs of the difference are smaller than 6 mm (~1 mm PWV), and the correlation coefficients are about 0.5 for different implementation approaches. Above comparison results in the work provide a quantitative extent to which atmospheric measurements from GPS and SAR APS are comparable. Another significant finding is that in most cases the STD of difference (between GPS and SAR APS) is slightly smaller than STD of SAR APS itself in both comparison modes. It implies the potentiality to correct atmospheric errors in SAR interferometry with high-precision GPS meteorological products, i.e. tropospheric delay or water vapor.

1. Introduction

Spatial and temporal variations of the atmosphere, e.g. pressure, temperature and water vapor content, directly result in atmospheric refractivity heterogeneity and then produce atmospheric artificial phases on SAR interferometry during the propagation of radar signals through the air. Such atmospheric induced artificial phases can be a limiting factor of high-accuracy measuring on subsidence deformation monitoring with InSAR. Zebker et al. reported that 20% spatial or temporal change in relative humidity could result in 10–14 cm deformation error for baselines ranging from 100 m to 400 m in the case of SIR-C/X SAR (Zebker, 1997).

In the last decade, various approaches were proposed to model and mitigate the artificial phase due to atmospheric heterogeneity. These approaches can be classified into two groups. The first group detects temporally stable interferometric points using time series of SAR images and spatially filters out such atmospheric phases among detected stable points. Typical algorithms including this approach are PS-InSAR (Ferretti, 2000, 2001), SBAS (Lanari, 2004). The other one models the InSAR atmospheric effect (mainly the water vapor effect) with external water vapor measurements, e.g., GPS Precipitable Water Vapor (PWV) (Bevis, 1992; Williams et al., 1998), MODIS/MERIS (near) infrared water vapor product (Gao, 2003; Li, 2005, 2006b), predicted water vapor products from Numerical Weather Prediction (NWP) models (Wadge, 2002; Jade, 2008), Radiosonde profiles. Among them,

* Corresponding author. Tel.: +852 6500 1343.
E-mail address: daniele.perissin@cuhk.edu.hk (D. Perissin).
[1] Fok Ying Tung Remote Sensing Science Building, CUHK, Shatin, New Territories, Hong Kong.

1364-6826/$ - see front matter © 2012 Elsevier Ltd. All rights reserved.
http://dx.doi.org/10.1016/j.jastp.2012.06.005

independent GPS zenith delays or the water vapor retrieved from regional Continuous Observation Reference Systems (CORS) (Li, 2004; Li, 2006a; Xu, 2006; Cheng, 2009) were the most widely used.

In the last ten years, several case studies have introduced how GPS derived Zenith Wet Delay (ZWD) or PWV can be used in atmospheric correction of InSAR. Williams et al. assessed the possibility of reducing atmospheric effects on SAR interferograms using Southern California Integrated GPS Network (SCIGN) GPS data through simulation (Williams et al., 1998). A comparison between GPS zenith delays estimated from a 14 GPS permanent stations network and InSAR measurements was performed over Mt. Etna. The result showed that the equivalent values for InSAR-GPS gave an RMS value of 19 mm with a mean of +12 mm (Wadge, 2002). Li et al. employed GPS data in SCIGN to develop the GTTM model for InSAR atmospheric mitigation, especially the height dependent and long-wavelength atmospheric terms (Li, 2006a). However, fully investigations were rarely reported on the agreement between accurate InSAR atmospheric phases and GPS derived atmospheric measurements. Therefore, there is a demand for drawing a reliable conclusion on performance of InSAR atmospheric correction with GPS data.

To overcome the deficiency of previous studies, an agreement analysis between GPS and SAR was conducted through a comprehensive comparison between GPS zenith delay and SAR Atmospheric Phase Screen (APS) with a novel comparison methodology. Section 2 describes both spatial and temporal coverage of ENVISAT ASAR data (both ascending and descending) and GPS campaign data. Section 3 introduces the methodology of comparison with consideration of the different characteristics of SAR APS and GPS delay. In Section 4 height sensitive stratification of APS and the determination of stratified ratio are specifically studied for the subsequent comparison of the mixing turbulence component. In Section 5, based on the comparison methodology and the stratification sensitivity analysis, the total atmospheric delay, the stratification component and the turbulence component (after removal of the spatial linear trend and stratification) from GPS and SAR APS (ascending and descending respectively) are compared in both differential mode and pseudo-absolute mode. Conclusions are presented in the last section.

2. Experimental scheme and data set

In order to quantitatively analyze the agreement between GPS atmospheric measurements and InSAR correspondents, an experiment of comparison between GPS zenith delay and SAR atmospheric phase was designed. The data collection in this experiment was realized as part of the METAWAVE (Mitigation of Electromagnetic Transmission errors induced by Atmospheric Water Vapor Effects) project funded by ESA (European Space Agency). SAR images time series and local GPS campaign observation data for the experiment were collected in Como, Lombardy, in the northern part of Italy.

The ENVISAT ASAR images were acquired in two selected tracks, the ascending track 487 and the descending track 480. The map of each track and the overlapping coverage of the two tracks are shown in Fig. 1. The dates of data acquisitions for the two tracks are shown in Fig. 2. In total, 38 plus 28 ENVISAT ASAR images were available for this experiment during the period 2003–2008 for the track 487 and the track 480 respectively. The SAR image on date 20070715 was adopted as master for both tracks in the PSInSAR analysis. In this experiment, the Atmospheric Phase Screen (APS) for each SAR acquisition was estimated from SAR time series imagery with PSInSAR technique (Ferretti, 2001) and the Matlab tool SARProz (Perissin and Ferretti, 2007; Perissin, 2008). APS of two SAR tracks were processed independently.

GPS observations were collected for about six months throughout the GPS campaign from a local GPS network in Como with an area smaller than the SAR coverage; this area is shown by the black rectangular box in the left figure of Fig. 1. Eight GPS stations were installed in the Como test site at different distances (ranging from about 10 km, 1 km to 100 m). The right figure in Fig. 1 sketches the location and distribution of the GPS stations in Como. However, only the data of six days were partially synchronous with SAR acquisitions, as marked by black circles in Fig. 2. Moreover, three of the eight stations were inoperative on four of the six days.

GPS data at a 5 min interval was processed with the BERNESE package with precise IGS orbits. For the stations operating well,

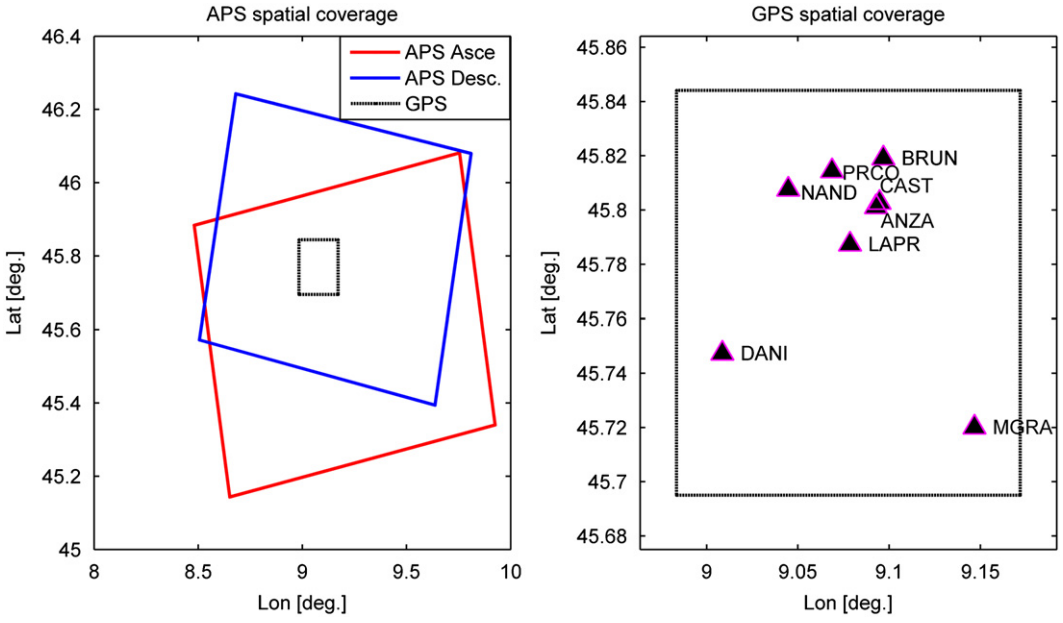

Fig. 1. Map of SAR imagery and GPS data. Left: Red and blue rectangular boxes give the spatial coverage of SAR imagery for ascending and descending tracks, respectively. Right: Locations of GPS stations in Como, Italy, which are marked with black triangles. (For interpretation of the references to colour in this figure legend, the reader is referred to the web version of this article.)

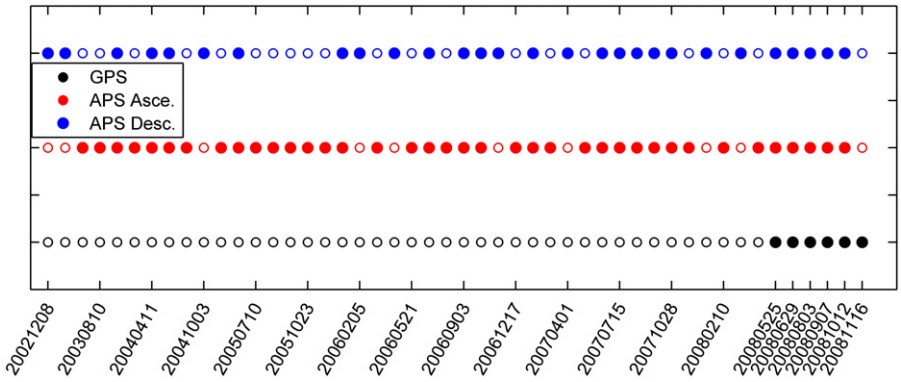

Fig. 2. Time series of ENVISAT ASAR imagery and GPS datasets. Filled circles indicate that synchronous data are available on the listed date. Circles in black, red and blue stand for datasets of GPS, ascending SAR and descending SAR, respectively. (For interpretation of the references to colour in this figure legend, the reader is referred to the web version of this article.)

Table 1
Temporal list of GPS dataset at all stations for Como, Italy.

Stations\Date	20081116	20081012	20080907	20080803	20080629	20080525
ANZA	25	25	25	25	25	25
BRUN	25	25	25	25	25	25
CAST	25	25	25	25	25	25
DANI	25	25	NaN	NaN	NaN	NaN
LAPR	25	25	25	25	25	25
MGRA	25	25	NaN	NaN	NaN	NaN
NAND	NaN	25	NaN	NaN	NaN	NaN
PRCO	25	25	25	25	25	NaN

hourly GPS zenith delays were retrieved under piece-wise linear model from GPS phase observations. Totally 25 samples of Zenith Total Delays from 00∼24 UTC were stacked on each operational station per day. Table 1 gives the available samples of zenith delay of GPS dataset in this experiment. Available hourly samples per day for each station are given in the table. NaN means that data values are unavailable on that day for the station.

3. Comparison methodology

In order to compare SAR APS with GPS delays to test their consistency and agreement, differences of atmospheric correspondence from both dataset are firstly stated. Considering above differences, data conversion and synchronization are then implemented correspondingly to derive comparable values with consistent spatial and temporal characteristics. Finally all scatter points of SAR APS sparse dataset and overlapped GPS delays on the same date (pair of dates) are compared in differential mode and 'pseudo-absolute' mode.

3.1. APS by PS-InSAR

With recently developed PS-InSAR technology (Ferretti, 2001), the Atmospheric Phase Screen (APS) can be derived along with the local deformation rate and residual ground height on a sparse set of interferometric stable points from multiple interferograms. The algorithm is implemented through two main steps (Perissin, 2010). Firstly, relative height and deformation trend are inversely searched from temporal phase series of connections of neighboring PSC's selected using an amplitude stability index. The second step is the integration of the small atmospheric contributions of unwrapped phase through the spatial graph of reliable PS's for each interferogram.

To compare the atmospheric propagation delay in troposphere (atmospheric delay for short in the following) in APS with atmospheric delay retrieved by other independent techniques, we further regard the spatial atmospheric signal as being composed of the following four parts: a spatially linear plane trend, a height dependent stratification term, a spatially correlated perturbation term, and a ground feature dependent part. The atmospheric signal as a function of space coordinates$x$and$y$ (in range and azimuth directions) can then be written as follows (Perissin, 2010):

$$\alpha_i(x,y) = a_i + b_i x + c_i y + \varepsilon_i(x,y) + k_i \cdot h(x,y) + w_i \cdot z(x,y) \quad (1)$$

In the equation, $\alpha_i(x,y)$is the atmospheric phase (or delay) at temporal epoch i at spatial point with 2D radar coordinates (x,y). $a_i + b_i x + c_i y$ is a spatially plane trend; $k_i \cdot h(x,y)$ is the height dependent stratified term, in which k_i is phase (or delay) to height ratio. $\varepsilon_i(x,y)$ is the spatially correlated perturbation term, in which most of the signal is from the atmospheric turbulent processes. The last part $w_i \cdot z(x,y)$, stands for the ground feature dependent term, e.g., the land cover, water body etc., and w_i indicates the weight of influence of the ground feature$z$ (x,y). The above model is adopted in our analysis based on following reasons: firstly, turbulence term and stratification in the total atmospheric delay are the most important components being concerned (Hanssen, 2001); secondly, spatial liner trends would inevitably bring systematic errors in the comparison due to imperfect modeling of satellite orbits, which cannot be neglected. Employing the model in Eq. (1), we intend to compare specific signal components between GPS and SAR APS, instead of mixed signals in total as conventional ways.

3.2. PWV retrieved from GPS meteorology

Similar to SAR interferometry, GPS measurements are subjected to propagation delays due to atmospheric refractivity when

the microwave signal transmits through the air (both troposphere and ionosphere). Such propagation delays are used to inversely retrieve the amount of Zenith Wet Delay (ZWD) or Precipitable Water Vapor (PWV), provided that hydrostatic term in troposphere could be accurately modeled and ionospheric effect can be precisely compensated. The implementation of this concept is named 'GPS meteorology' (Bevis, 1992). Based on above concept, properties of PWV retrieved from GPS are summarized as follows:

1) *Spatially average within an inverted cone*
   GPS water vapor is an averaged quantity in an inverse cone, the boundary of the inverse cone being dependent on the maximum zenith angle of GPS observations. Final PWV is projected from each slant angle into zenith direction with a least squares adjustment. Niell Mapping Function (NMF) with 1st order horizontal gradient is adopted in this data preparation (Niell, 1996; Herring, 2006).
2) *Absolute measures*
   PWV estimated from GPS is the total amount of water vapor along a vertical profile from ground to the upper air. These PWV's are spatially absolute measuring values. This can be realized either by a Precise Point Positioning (PPP) strategy or by a differential positioning strategy with introducing a reference station whose PWV values are determined with respect to a reference regional network.
3) *Temporal independence*
   GPS water vapor is also temporally independent, which means water vapor amount in different epochs of time series have no correlation. Each node of PWV time series is significant and independent in adjustment or statistics; this provides a tool to analyze the variation law of water vapor in the time domain.

3.3. Comparison implementation

APS products derived from PSInSAR are differential measures which are temporally relative to a master image and spatially related to a reference point, while water vapor values estimated with other techniques (e.g., microwave radiometers, radiosondes, GPS, MERIS, MM5 etc.) are absolute measurements. The difference of their temporal characteristics restricts direct comparison between SAR APS and GPS water vapor. In front of this reason, their temporal disagreements are resolved at first step.

In this paper we propose to transform GPS delays into differential values or to recover the SAR APS in absolute values, and then to compare two data sets in differential or absolute way correspondingly. According to the temporal domain of comparable values, we classify the comparison into two modes: the differential mode and the absolute mode. The comparison in differential mode was implemented by subtracting GPS Zenith Tropospheric Delay (ZTD) at master acquisition time from the original GPS delays. A differential operation within a pair of two dates (synchronized to GPS) on APS is required to cancel out the common unknown atmospheric delay at master time if the master of APS in PS-InSAR was not covered by GPS data series. The concept of absolute comparison is to estimate SAR atmospheric delay at master time from GPS time series and then to compensate all SAR APS for approximately estimated delays. Finally recovered SAR APS are compared with GPS in the absolute domain. Because that SAR atmospheric delay at master time cannot be genuinely recovered from GPS, comparison in this mode is called 'pseudo-absolute' comparison.

To obtain comparable values of two datasets, besides the unification of temporal reference as illustrated in above two modes, additional disagreements must be considered and correspondingly resolved as follows.

(1) Radar slant phases are projected into zenith delay. Considering that GPS ZTD's are given in one-way vertical direction while the radar APS are expressed in slant two-way phases, a mapping function of the incidence angle is accounted for to project radar APS into zenith delay. A cosine function was adopted to project the radar phase in line of sight to vertical delay for simplifying, as illustrated in Eq. (2) (Cheng, 2009):

$$\varphi(\mathrm{APS})_{LOS}^{2way} = \frac{ZWD \cdot 4\pi}{\lambda \cdot \cos(\theta_{inc})} \tag{2}$$

In Eq. (2), λ is wavelength of radar, and θ_{inc} indicates the local incidence angle. With above projection and transformation, the comparable atmospheric delay in mm is presented for both SAR APS and GPS delay in the following context if no additional specifications are given.

(2) ZTD, ZWD and PWV are linked and unified in comparison. In the case of spatial or temporal differentiating, the difference between ZWD and ZTD can be neglected. Meanwhile, with a locally constant scale factor, ZWD keeps a directly linear relationship with PWV. Therefore, ZTD, ZWD and PWV are linked in the paper. The three terms are unified into ZTD for comparison and analysis in next sections.
(3) Geo-coded SAR APS are resampled into GPS locations. With this data handling, SAR APS are registered into WGS84 geographic system and then interpolated into GPS locations before point-based comparison. If the data of one GPS station are unavailable for a given day, the interpolation at this station on the given day is neglected.
(4) Spatial linear trends are removed from APS. The residual phases due to inaccuracy of satellite orbit modeling are inevitably encompassed into APS as systematic errors, which behave as a spatial liner trend on interferograms (Hanssen, 2001). Therefore a linear phase trend is removed from each APS. Theoretically it is required to remove spatial linear trends from GPS to keep consistency with APS, but we gave up this intention when considering the following two reasons. The first one is that GPS atmospheric delays on Como stations are spatially independent because a wide GPS reference network is introduced in processing. The second is that it can highly possibly lead to instability in estimation of spatial trends with a limited number of GPS stations in our case.
(5) Arithmetic means are removed from GPS in space. SAR APS are spatially differential values, referring to a reference point. In order to keep consistency with APS, we remove the spatial average of GPS samples to cancel out the unknown bias between GPS delays and differential APS.

4. Height sensitive stratification of APS

Height dependent stratification has been already identified as one influential component of the atmospheric effect on SAR Interferograms (Hanssen, 2001). However, systematic analyses of such stratification effect on APS products, as well as comparisons of such stratification effect between APS and corresponding atmospheric products from other sensors have not been performed yet. To compare the components of stratification and the assumed turbulence between GPS and SAR APS, different components must be clearly discriminated in advance. This section focuses on the analyses of stratification effect on APS. As illustrated in last section, the spatial linear trend, the stratification term, and the turbulence term coexist in SAR APS. Therefore, a

robust method must be given to derive stratified ratios of APS from original APS scatter points.

In this section, we introduce a method with following steps to estimate APS stratified ratios with improved reliability. At the first step, original APS values are divided into even groups according to the height of PS points. And then statistical means and standard deviations within each group of APS values are calculated. Furtheremore, curves of statistical numbers versus height for grouped APS values are plotted. Contributions of different components of APS are discriminated based on their individual characteristics presented on these curves. Finally, ratios of phase to height are regressed from the APS samples representative of stratification effect only.

The above method is realized in the following ways and illustrated with experimental results as follows. As the first way, one-way zenith delays of original APS against height for each day are plotted to discriminate their height dependent characteristic of different APS components: a spatial linear trend, the turbulence and the stratification. It can be observed that linear trends of atmospheric delays related to elevation dominates in scatter points of original APS delays, especially in the ascending cases (stands for in blue color in Fig. 3). These linear trends are named stratification effect based on theoretically physical definition. Besides above feature, it can also be perceived that trends of APS lower than certain height values are inconsistent with general ones and the statistical means as well as standard deviations of APS under this height remarkably differ than averaged ones, e.g., on all available days of descending track and on 20080629 of ascending track. This height, under which original APS points (blue color in Fig. 3) have a reversed tendency compared to APS points over it, hereafter is named as the critical height.

The critical height of 250 m was empirically fixed from our experimental data, which was marked with red vertical lines in both ascending and descending graphs (referring to Fig. 3). After plotting the APS under such the critical height, a spatial linear trend can be observed. Based on above experimental analysis and the knowledge in Section 2, the original APS (in blue color) under the critical height is assumed to be mainly affected by spatial linear trends caused by inaccuracy of SAR satellite orbits modeling. This assumption was further verified by the change of APS scatter points after removing such spatial linear trends (drawn in black color in Fig. 3). For scatter points after operation of removing

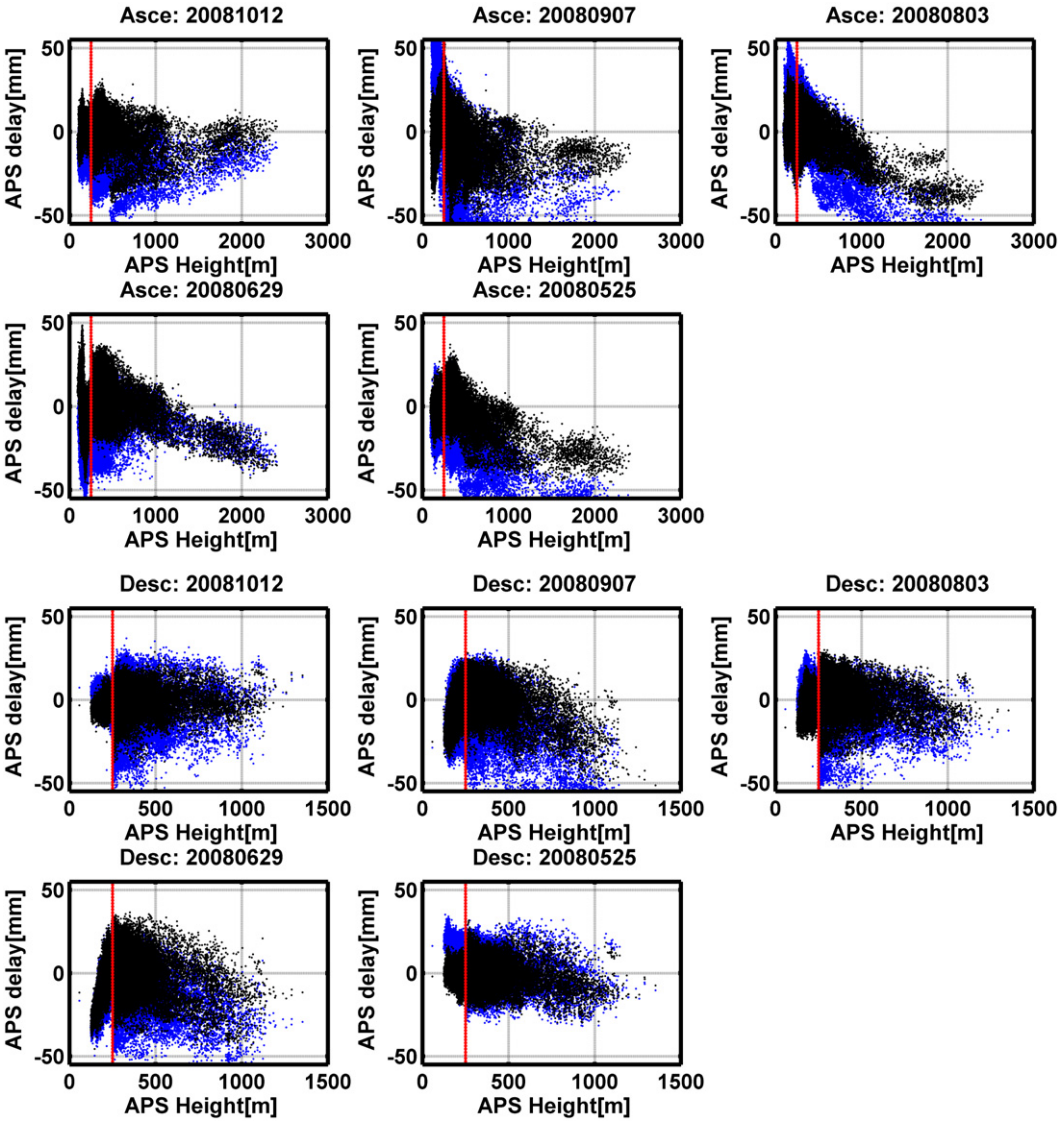

Fig. 3. One-way zenith delays of SAR APS against APS height for the dates synchronous with GPS. Top: Ascending track. Bottom: Descending track. The red vertical lines in all graphs show APS at a height of 250 m, for ascending and descending. Blue scatter points stand for original APS; Black points represent APS after removal of the spatial linear trend.

spatial linear trends, the dispersion of entire APS dataset decreased. In addition, the trend of APS under the critical height has been rectified (e.g., on 20080907 of ascending track), while the trend of APS over the height is kept unchanged. Therefore, based on our experimental analysis operated in the first way, APS points under the critical height are neglected in estimation of stratified ratios under the assumption of spatial linear trend.

As the second way, to further differentiate the effects of the stratification and the turbulence, APS scatter points were divided into even groups based on their PS heights and statistical differences of above two components from consecutive grouped APS were observed. With our dataset, different width values of APS height in divided group were experientially tested with 3 cases. The width of APS height per group increased from 100, 160 to 250 m for the ascending, and from 60, 100 to 160 m for the descending respectively. It can be explained with the reason that the range of APS height in the ascending track is 2400 m, while the number in the descending track is 1400 m. For each case, the arithmetic mean, STD and number of samples were accordingly figured out from APS samples within each group. After the testing, we only show the results with group width of 160 m for the ascending and 100 m for the descending, due to that statistical curves among different cases are kept with little difference. Fig. 4 plots the arithmetic mean, standard deviation and a quarter of range (1/4 of difference between Max. and Min.) of grouped APS. The height of all grouped APS points joining calculation began from 250 m. APS samples with the height under 250 m were discarded here with intention of removing the spatial linear trend.

From Fig. 4, the quatered range and standard deviation of grouped APS decreases and the number of grouped APS samples exponentially decreases along with the increase of APS heights for both tracks. Moreover, it can be observed from the curves that grouped APS has large variations at the "head" and high sparsity at the "tail" of the curves. Specifically, the quartered range and the standard deviation of grouped APS with smaller heights (from 250 to 850 m for ascending and from 250 to 550 m for descending) is higher than that with larger heights. Meanwhile, APS data with larger heights (beyond 2050 m for the ascending and 1150 m for the descending) have samples less than 100. Under this context, the former phenomenon was primarily interpreted as mixing turbulence effect which strongly dominated in lower elevations under the height minmum. We regarded this effect as 'Head Effect' that turbulence dominated APS signals in low height. While, the latter one was regarded as 'Tail Effect' because that few number of APS samples beyond the height maxmum restricted the reliablity of stratification estimation. From the above analysis, components, APS samples due to the effect of spatial linear trends, the 'Head effect' and the 'Tail effect' were

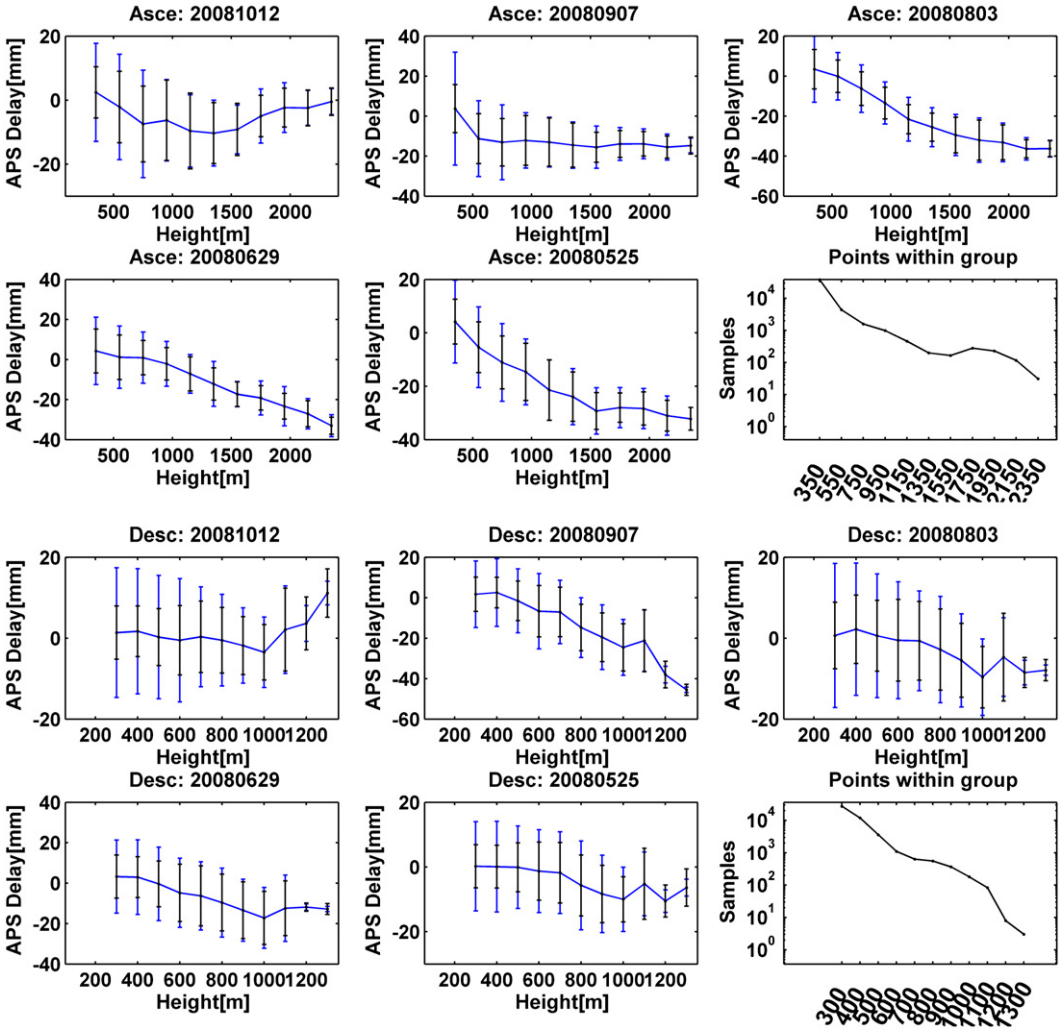

Fig. 4. Mean, standard deviation error (in black) and a quarter of range (in blue) of grouped APS delay after removal of spatial linear trend. Each group is determined by APS height, which increased in steps of 200 m for ascending and 100 m for descending. The solid black dotted line is added in the last sub-graph to represent the total sample numbers in each APS group. (For interpretation of the references to colour in this figure legend, the reader is referred to the web version of this article.)

removed in the final estimation of stratified ratios for a more reliable solution. Such APS stratified ratios obtained from samples affected by stratification effect only are then taken in the comparison analysis in the next section.

5. Results and discussions

This section demonstrates comparison results of the zenith delay between GPS and SAR APS. Comparison results in differential mode and pseudo-absolute mode are given respectively. With APS stratification analysis introduced in Section 4, stratification components and regressed stratified ratios from SAR APS products are particularly compared with that from GPS in differential mode firstly. In two comparison modes, atmospheric delays from SAR APS and GPS are compared at three consecutive stages at which each APS component within the model given in Section 3.1 is sequentially separated. Finally STD's of GPS, STD's of SAR APS and STD's of differences between both were listed to show their individual dispersion and the consistency between GPS and APS.

5.1. Differential mode

As described in Section 3.3, in the differential comparison mode, we transformed absolute GPS delays into spatial and temporal differential values and then made comparisons with SAR APS in the differential domain. Totally 10 differential APS pairs were generated with random combination from 5 SAR images for each track which are synchronous with GPS (referring to Fig. 2).

5.1.1. Comparison of stratified ratios

The sensitivity of stratified ratios on the APS height in regression under the mixture of a spatial linear trend and a turbulence term were analyzed in Section 4. In differential mode, the estimated

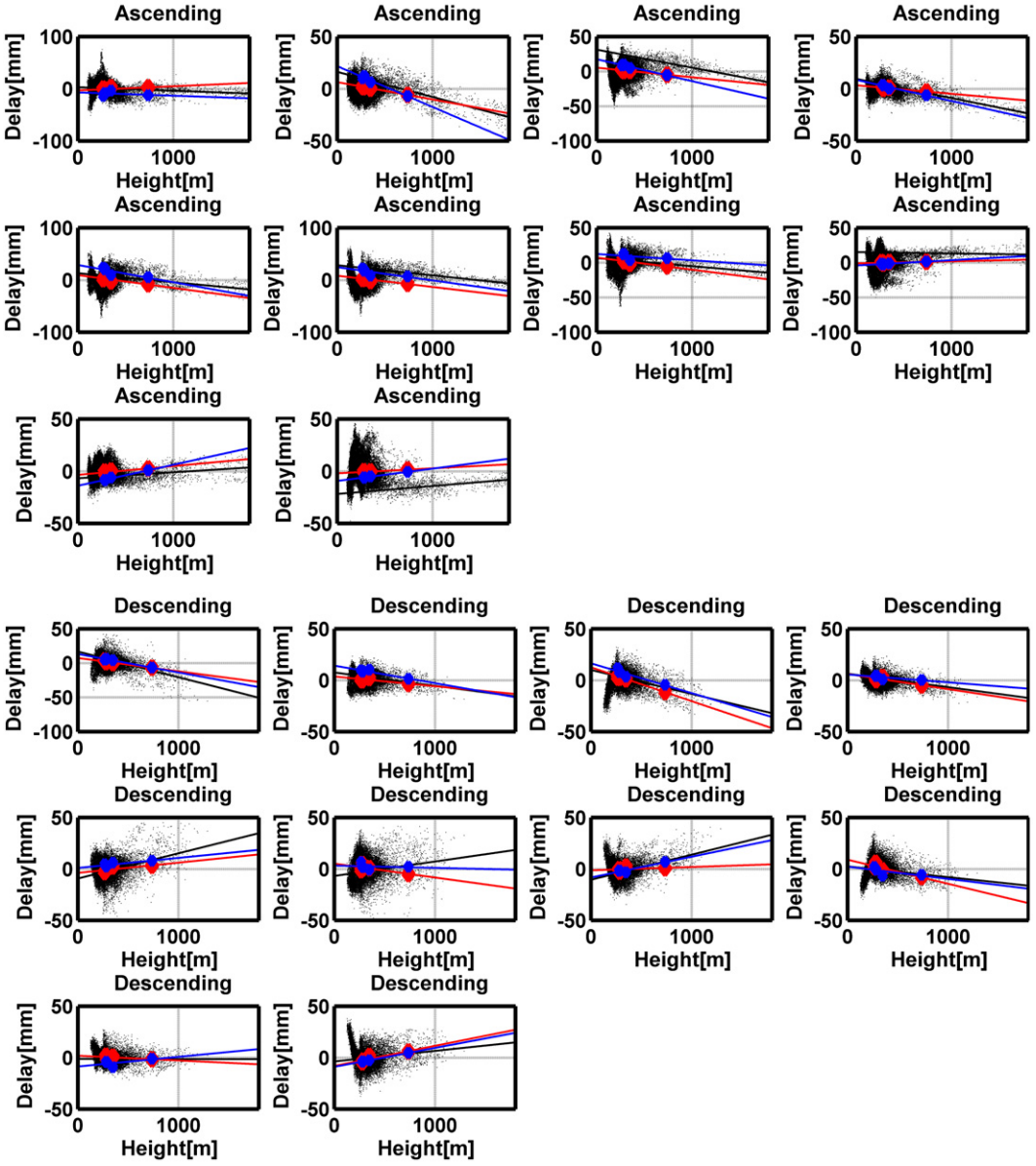

Fig. 5. Atmospheric delay against height for original SAR APS and original GPS ZTD. Ascending (Left) and descending (Right). In both sub-graphs, the black color is for original SAR APS values, blue symbols stand for the interpolated APS points geographically overlapped with GPS stations, while the GPS delay are plotted in red. Fitted lines by linear regression are plotted to represent their estimated stratified ratios. (For interpretation of the references to colour in this figure legend, the reader is referred to the web version of this article.)

ratios of delay to height were compared between GPS delay and SAR APS with a linear stratification assumption. In addition, correlation coefficients and STD's of estimated stratified ratios between these two data sets were listed to quantitatively give their consistency.

In Fig. 5, scatter plots of delays on height are plotted for two datasets (in both ascending and descending track). In the Figure, the black color stands for original SAR APS values, blue symbols stand for the interpolated APS points geographically overlapped with GPS stations, while the GPS delay are plotted in red. Fitted lines by a linear regression are plotted to represent their estimated stratified ratios. Fig. 5 provided a direct perspective of atmospheric delay against ground height. From Fig. 5, stratification slopes given by lines in three colors are close to each other. Moreover, compared to interpolated APS points, strarification slopes regressed from whole APS scatter dataset is more close to slopes from GPS stations which indirectly demonstrates the need of statistical stratification analysis from grouped APS.

With a higher reliability, stratified ratios regressed from whole APS scatter dataset were kept in statistical comparisons. Estimated stratified ratios from the original GPS delays and from the original SAR APS are plotted in Fig. 6. Meanwhile, statistical correlation coefficients and STD's of estimated stratified ratios are listed in Table 2. We found from the table that APS and GPS have comparable stratification ratios. The estimated stratification ratios from both datasets coincide with each other with a correlation coefficient of more than 0.7, but the ascending track has a higher coincidence than the descending one. The bias and standard deviation of differences of stratification ratios between GPS and SAR APS in ascending (3.4 and 7.7) are much smaller than that in descending (6.1 and 13.9). Higher amount of water vapor in the morning (at UTC 09:43, i.e.08:43 a.m. in Rome, Italy for descending track) were expected to introduce stronger atmospheric decorrelation and then higher dispersion in the interferometric phase for descending SAR data, as mentioned in Section 4. For the ascending data, the statistics given in Table 2 imply discrepancies with a bias of 0.55 mm and a STD of 1.24 mm for water vapor in 1 km height range between GPS delay and SAR APS based on experimental data and proposed manipulation.

5.1.2. Comparison of atmospheric delays

In this section, we compared the atmospheric delay in three stages. The first one is the total delay. The second stage is the delay after removing of the spatial linear trend. The last stage is the delay after removing of the spatial linear trend as well as height dependent stratification which were estimated in the last section. The residual delays at the last stage are regarded as turbulence delay since residual signals are mostly caused by turbulence effect after removing the spatial trend and compensating stratification components according to the assumption of our model in Section 3.1. The comparison results in above three stages are given in Figs. 7–9 respectively. Furthermore, we integrate all samples of comparable values on each pair of dates and made the following statistics: STD of GPS, STD of SAR APS, STD of difference between both, correlation between two series, the slope of APS delay on GPS. Above statistics in different stages are listed in Table 3.

We found the following phenomena from scatter points from Figs. 7–9 and indexes from Table 3:

1) On the stage of total delay in the first row, after the removal of individual averages, and without any additional operations, the GPS delay and SAR APS agree with each other in differential mode with the standard deviation of the difference being less than 4 mm and the correlation coefficient being higher than 0.6.
2) On the stage of turbulence and stratification delay in the second row, after removal of the spatial linear trend in the original APS, the consistency between the two datasets is stronger, with higher correlation and smaller standard deviation.
3) In the third row, after removal of both linear trends and height dependent stratification components, the assumed atmospheric turbulence components from GPS and SAR APS are moderately correlated with a coefficient near to 0.5, while the standard deviation of difference decrease to less than 3 mm for the both tracks.

To summarize the comparison in differential mode, some general laws can be drawn from Figs. 7–9 and corresponding

Table 2
The statistics of stratification ratios from GPS delay and SAR APS. Unit: mm/km.

APS vs. GPS	Corr. Coef	Bias	STD Diff.	Slope	Intercept
Ascending	0.81	3.39	7.73	0.76	−5.29
Descending	0.74	-6.11	13.92	0.96	5.73

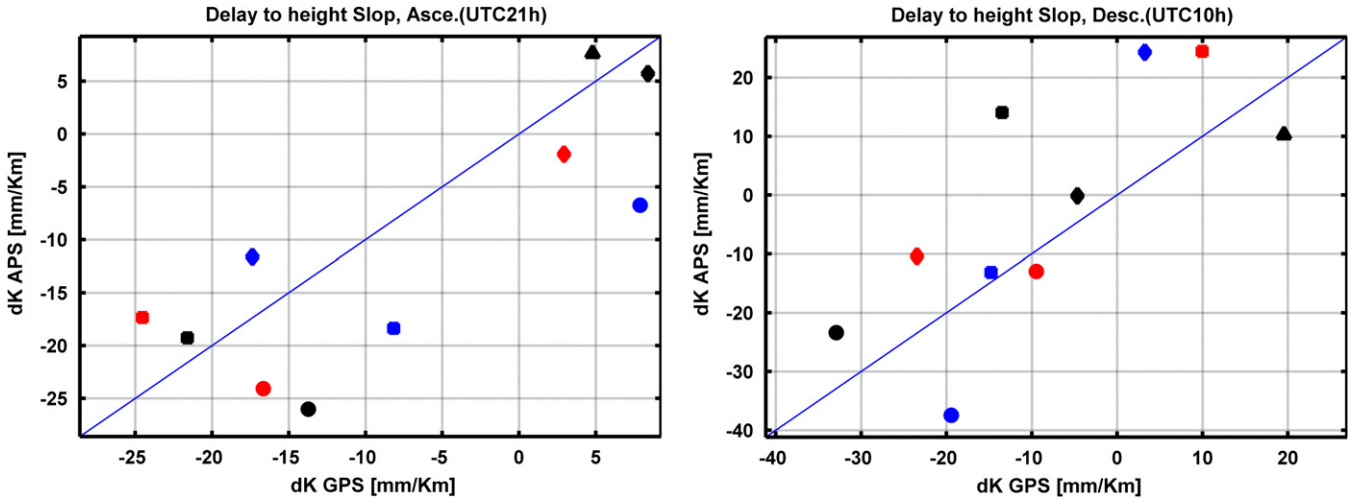

Fig. 6. Cross plot of estimated stratified ratio from the original GPS ZWD and the original SAR APS. In the upper sub-graphs, the stratified ratios are estimated from the original SAR APS. (Left) ascending and (Right) descending pass. Unit of the stratified ratio is mm/km.

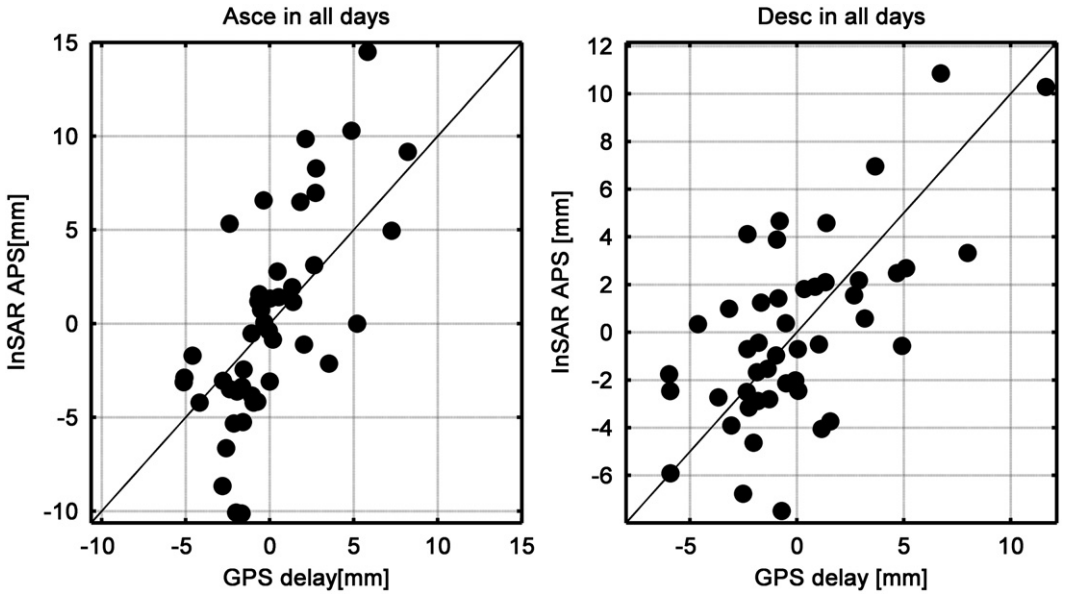

Fig. 7. Cross Plot of zenith atmospheric delay (Total delay) between GPS and SAR on all temporal pairs in the differential comparison. (Left): Ascending track. (Right): Descending track. Individual spatial averages at available overlapping stations for both datasets are removed for comparative demonstration.

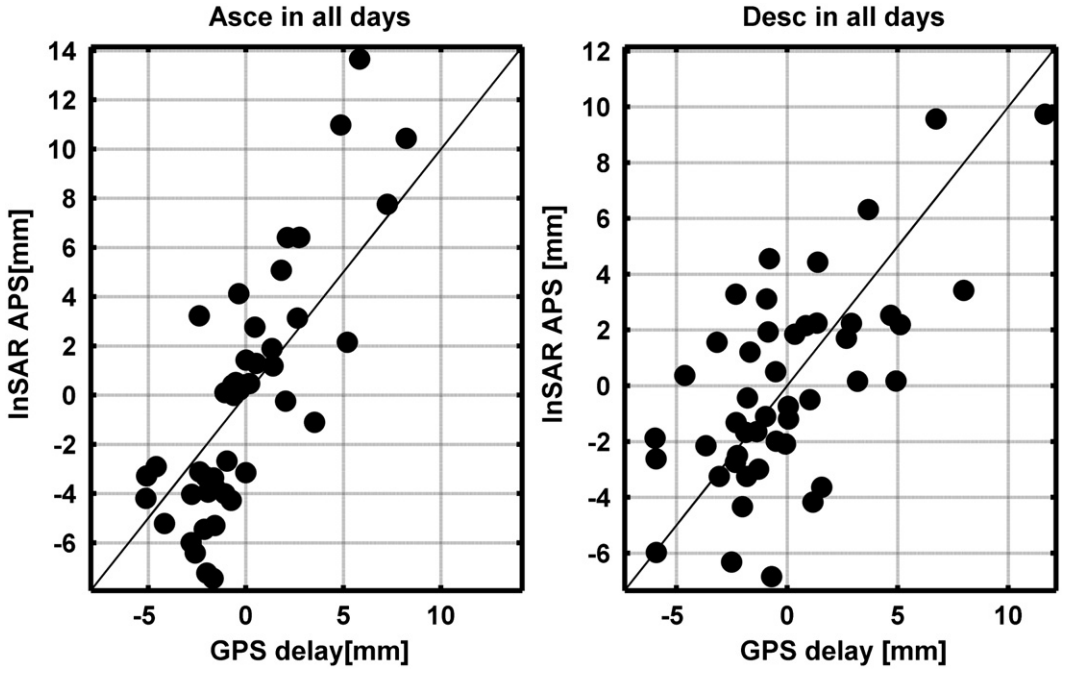

Fig. 8. Cross Plot of zenith atmospheric delay (after removal of spatial linear trend) between GPS and SAR on all temporal pairs in differential comparison. (Left): Ascending track. (Right): Descending track. Individual spatial averages at available overlapping stations for both datasets are removed for comparative demonstration.

numbers in Table 3. Agreement between GPS delay and SAR APS generally holds in most cases. For the original total delay (or only including stratification and turbulence), dispersion of GPS is smaller than that of APS itself. With the help of GPS zenith delay, APS noises can be reduced at a certain extent by a differential (between GPS and APS) operation. Even for only assumed turbulence, with the height sensitivity analysis of stratification in Section 4, turbulence delay from GPS can still be possibly employed to mitigate the turbulence signal from APS, which could be evidenced by the change of STD (2.95 for STD of APS to 2.60 for STD of difference) in SAR ascending track. (Figs. 8 and 9).

For the ascending track, the reasons for the decrease in correlation are: (1) The stratification ratio estimated from GPS and SAR APS has a standard deviation of more than 7 mm/km, as shown in the last section; (2) 7 of 8 GPS stations are located at lower heights, but the stratification term on APS is removed on all the APS scatter dataset. When APS are interpolated on GPS stations, the removal of the linear trend on all APS may introduce artificial model error on interpolated APS points because that 7 of 8 stations are at lower height. The decending track shows no correlation for the turbulence term between both; this is because of the large RMS error in the APS data itself, and the uncorrelated stratification ratio-the STD differences in ratios are at about 14 mm/km.

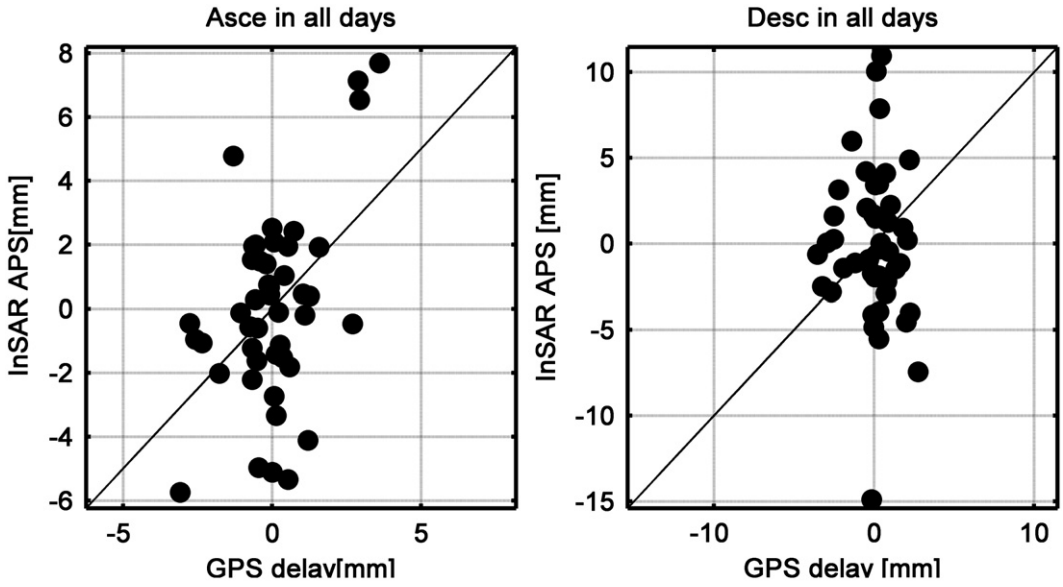

Fig. 9. Cross Plot of zenieth atmospheric delay (turublence delay) between GPS and SAR on all temporal pairs in differential comparison. (Top): Ascending track. (Bottom): Descending track. Linear spatial trend and stratification effect are removed from the original APS, stratification on GPS stations are removed for comparable demonstration. Individual spatial averages at available overlapping stations for both datasets are removed.

Table 3
Statistics of differential comparison between GPS and SAR APS at two stages. Unit: mm.

Atmospheric delay (10 Pairs)	Ascending					Descending				
	STD GPS	STD APS	STD Diff.	Corr. Coef.	Slope (APS V. GPS)	STD GPS	STD APS	STD Diff.	Corr. Coef.	Slope
Total delay	3.02	5.44	3.99	0.69	1.25	3.58	3.86	3.16	0.64	0.69
Turbulence delay and stratificaiton	3.02	4.99	3.09	0.81	1.34	3.58	3.62	2.99	0.66	0.66
Turbulence delay	1.39	2.95	2.60	0.47	0.99	1.71	2.12	2.94	−0.16	−0.20

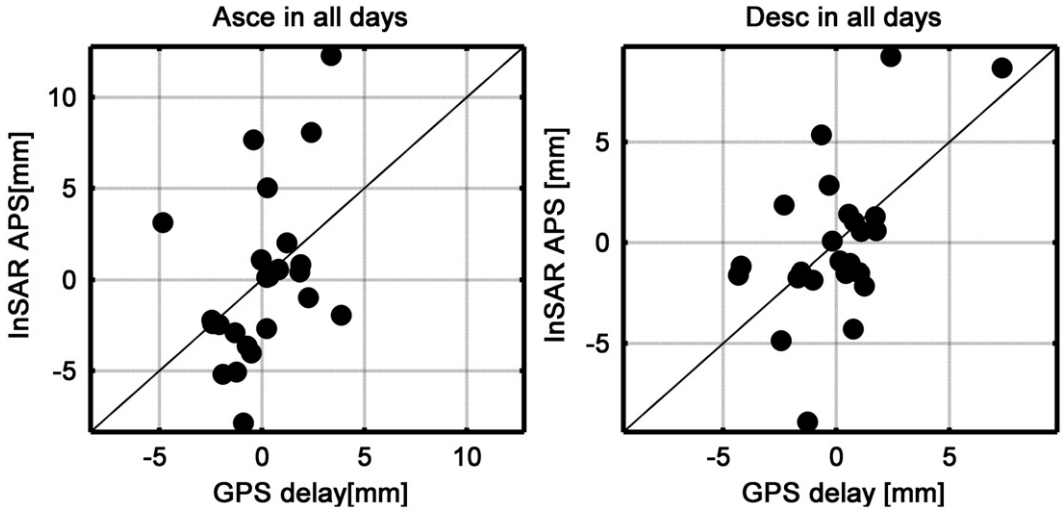

Fig. 10. Cross plot of zenieth atmospheric delay between GPS and SAR in pseudo-absolute comparison. While different from Fig. 8, the SAR master delay was estimated with the average of all GPS data and subtracted from the GPS series. (Left): Ascending case. (Right): Descending case. Individual spatial average at available overlapping stations for both datasets is removed for comparative demonstration.

5.2. Pseudo-absolute mode

The first implemented approach of the pseudo-absolute comparison was to estimate the SAR atmospheric delay at master time as an average of all GPS temporal series data (all hours within all days). The second implemented approach of this pseudo-absolute comparison included the following steps: first extracting GPS ascending and descending time series (synchronous with SAR APS) according to their passing time respectively, and then estimating the SAR atmospheric delay at master time by averaging of synchronous GPS temporal series. In this pseudo-absolute mode, after the obtaining of master delay, then the successive step of subtracting the master delay from GPS delay series was executed.

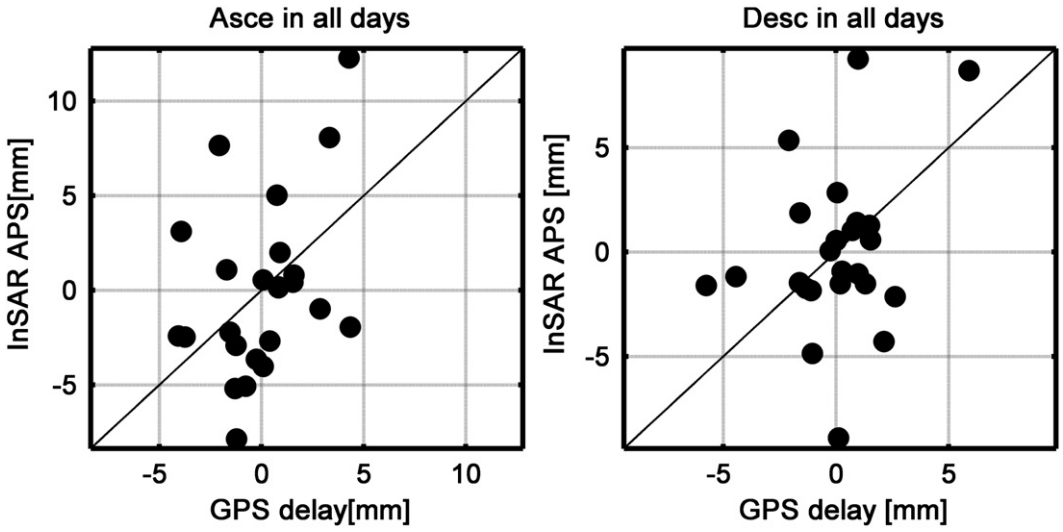

Fig. 11. Cross plot of zenieth atmospheric delay between GPS and SAR in pseudo-absolute comparison. SAR master delay was estimated with the average of synchronous GPS data and subtracted from the GPS series; individual spatial means were both removed. (Left): Ascending case. (Right): Descending case. Individual spatial averages at available overlapping stations for both datasets were removed for comparative demonstration.

Table 4
Statistics of pseudo-absolute comparison between GPS and SAR APS for total zenith delay.

Absolute mode Total delay (all 5 days)	Ascending				Descending			
	STD GPS	STD APS	STD Diff.	Corr. Coef.	STD GPS	STD APS	STD Diff.	Corr. Coef.
All GPS	2.03	4.65	4.26	0.40	2.36	3.91	3.28	0.55
Synch. GPS	2.33	4.65	4.37	0.37	2.31	3.91	3.94	0.28

Table 5
Samples of GPS in SAR master estimation in pseudo-absolute comparison between GPS and SAR APS.

Average on station		ANZA	BRUN	CAST	DANI	LAPR	MGRA	NAND	PRCO
Average of all GPS	Asce.	150	150	150	50	150	50	25	125
	Dsce.	150	150	150	50	150	50	25	125
Average of synchr. GPS	Asce.	5	5	5	1	5	1	1	4
	Dsce.	5	5	5	1	5	1	1	4

Figs. 10 and 11 illustrate comparable atmospheric delays between GPS and SAR APS at different stages in the two different implementated approaches respectively where different colors stand for different available stations. A generally good correlation in total delay can be observed in both figures. While the correlations of assumed turbulence delay are decreased a lot. Similar to the differential comparison, we made statistics to quantitatively describe the relationship of atmospheric measurements between GPS and SAR APS (referring to Table 3).

Statistics for two implementation approaches of pseudo-absolute comparison between GPS zenith delay and SAR APS are included in Table 4. From Table 4, we can summarize the following points:

(1) Correlations in the pseudo-absolute comparison mode are not as high as those in the differential comparison mode because the recovered master is not the genuine SAR master delay but approximately estimated from the average of GPS series.
(2) STD of GPS data are evidently smaller than STD of APS. STD of difference between two datasets in pseudo-absolute comparison mode are slightly smaller than that of APS itself in most cases. Though with different implementation, deviation of difference between two datasets are kept at the same level with STD being less than 5 mm in all cases.
(3) Master delay estimation with the average of all GPS provides a better comparable result than averaged synchronous GPS, because the GPS samples for averages in our comparison are extremely plentiful (referring to Table 5), enabling reliable average values as a substitute of the SAR master delay, while the case of averaging synchronous GPS does not.

5.3. Discussion

The differential comparison mode is physically representative of difference between the two data sets. In the differential comparison mode, the original delay from APS and GPS in 10 differential pairs have correlations higher than 0.6 in both tracks. The correlation increases and the STD of difference decreases after the removal of the spatial linear trend. When considering and removing the stratification term, agreement between the residuals of GPS ZWD and SAR APS is distinctly decreased; this could be acceptable because of additional inconsistency of the stratification between both. Though the performance varies, the atmospheric delay between GPS and SAR APS coincides with the STD of difference smaller than 4 mm ($\sim$0.65 mm PWV) in different stages in the differential comparison.

Pseudo-absolute comparison results are also provided in this section. The pseudo-absolute comparison is only approximately implemented, which inevitably brings implementation errors, but it still provides an alternative vision. The agreement of atmospheric delay in pseudo-absolute mode was slightly worse than that in differential mode, which is reasonable because the nominal term and delay at SAR master time are just approximately estimated. For the two implementations of the pseudo-absolute mode, taking the master delay as the average of the entire GPS temporal series can enrol more data samples, and therefore provide a stable estimation. Due to the different physical nature of GPS and SAR, we cannot expect the stratification from GPS and APS to be totally correlated.

Another point from our results is that the ascending track provides reliable and comparable results and good evidence for

our motivation, while the descending track does not. The first reason for this is the large noise in the APS data themselves which were implied by that the dispersion of APS for ascending track is smaller than that for descending track (refer to Fig. 3); the second reason is that the height range of the descending track is much smaller (only 1100 m).

6. Conclusion

In this paper, the stratification effect of APS with a mixture of turbulence as well as spatial linear trend was analyzed and two comparison modes between GPS and APS were innovatively implemented. The first significant finding in this paper is that GPS ZWD is directly proved to be comparable with SAR APS. With height-determined grouped APS, after removing the spatial linear trend and neglecting mixed turbulence at lower heights, the stratified ratios of SAR APS derived in this experiment coincides well with that of GPS. Their ratios correlates with a coefficient higher than 0.8 with a bias of 3.4 mm/km as well as a STD of 7.7 mm/km in the ascending case in the differential comparison (GPS–APS). In the descending case, though APS data have stronger noises and a larger STD, stratified ratios achieve the correlation with a coefficient of 0.74.

A second significant finding in our investigation is that it is possible to correct atmospheric noises in SAR interferometry with high-precision GPS meteorological products. This was directly proved by the experimental results that the STDs of delay differences (between GPS and SAR APS) in most cases are slightly smaller than STDs of SAR APS itself in both comparison modes. STDs of difference are reduced if compared to that of SAR APS when GPS is introduced in differencing, except for the turbulence component in the descending track. This can be our further research for the improvement of the capability of interferometric atmospheric correction with GPS products, which not only depends on water vapor itself (e.g. its accuracy and spatial density) but is also related to spatially statistical modeling as well as other affecting factors (topography, ionospheric activities etc.).

Acknowledgement

This research study was supported by the Research Grants Council (RGC) General Research Fund (GRF) (Project Reference No. 415911) and Research Grants Council (RGC) Research Funding (Project Reference No. CUHK450210) of the HKSAR, China. The study is also supported by the Direct Grant project (No. 2020968) of Chinese University of Hong Kong and independent Scientific Research Project (No. 618-274092) of Wuhan University. The GPS data and SAR images collected in Italy in this research were supported by the METAWAVE ESA project (No. 21207/07/NL/HE). Prof. Sanso and Prof. Venuti of the POLIMI DIIAR Group are also appreciated for GPS data processing.

References

Bevis, M., Businger, S., Herring, T.A., Rocken, C., Anthes, R.A., Ware, R.H., 1992. GPS meteorology: remote sensing of atmospheric water vapor using the global positioning system. Journal of Geophysical Research 97 (D14), 15,787–15,801.

Cheng S., Lin H., Jiang L., Chen F., Zhao Q., 2009. SAR interferometry atmospheric mitigation from GPS water vapor retrieval in Hong Kong. 2009 Joint Urban Remote Sensing Event, 20–22 May, Shanghai, IEEE Published Proceeding, doi:978-1-4244-3461-9/09.

Ferretti, A., Prati, C., Rocca, F., 2001. Permanent scatters in SAR interferometry. IEEE Transactions on Geoscience and Remote Sensing 39 (1), 8–19.

Ferretti, A., Prati, C., Rocca, F., 2000. Nonlinear Subsidence rate estimation using permanent scatterers differential SAR interferometry. IEEE Transactions on Geoscience and Remote Sensing 38 (5), 2202–2212.

Gao, B.C., Kaufman, Y.J., 2003. Water vapor retrievals using Moderate Resolution Imaging Spectroradiometer (MODIS) near-infrared channels. Journal of Geophysical Research 108 (D13), 4389, http://dx.doi.org/10.1029/2002JD003023.

Hanssen, R.F., 2001. Radar Interferometry: Data Interpretation and Error Analysis. Kluwer Academic, Dordrecht, Boston.

Herring, T.A., et al., 2006. Gamit Reference Manual (Release 10.3). Cambridge: Massachusetts Institute of Technology.

Jade, S., Vijayan, M.S.M., 2008. GPS-based atmospheric precipitable water vapor estimation using meteorological parameters interpolated from NCEP global reanalysis data. Journal of Geophysical Research 113, D03106, http://dx.doi.org/10.1029/2007JD008758.

Lanari, R., Mora, O., Manunta, M., Mallorqui, J.J., Berardino, P., Sansosti, E., 2004. A small-baseline approach for investigating deformations on full-resolution differential SAR interferograms. IEEE Transactions on Geoscience and Remote Sensing 42 (7), 1377–1386.

Li, Z., Ding, X., Liu, G., 2004. Modelling atmospheric effects on InSAR with meteorological and continuous GPS observations:algorithms and some test results. Journal of Atmospheric and Solar-Terrestrial Physics 66, 907–917.

Li, Z., Muller, J.-P., Cross, P., Fielding, E.J., 2005. Interferometric synthetic aperture radar (InSAR) atmospheric correction: GPS, Moderate Resolution Imaging Spectro radiometer (MODIS), and InSAR integration. Journal of Geophysical Research 110 (B3), B03410, http://dx.doi.org/10.1029/2004JB003446.

Li, Z., Fielding, E.J., Cross, P., Muller, J.-P., 2006a. Interferometric synthetic aperture radar atmospheric correction: GPS topography-dependent turbulence model. Journal of Geophysical Research 111, B02404, http://dx.doi.org/10.1029/2005JB003711.

Li, Z., Fielding, E.J., Cross, P., Muller, J.-P., 2006b. Interferometric synthetic aperture radar atmospheric correction: medium resolution imaging spectrometer and advanced synthetic aperture radar integration. Geophysical Research Letters 33, L06816, http://dx.doi.org/10.1029/2005GL025299.

Niell, A.E., 1996. Global mapping functions for the atmosphere delay at radio wavelengths. Journal of Geophysical Research 101 (b2), 3227–3246.

Perissin, D., Ferretti, A., 2007. Urban target recognition by means of repeated spaceborne SAR images. IEEE Transactions on Geoscience and Remote Sensing 45 (12), 4043–4058.

Perissin, D., 2008. Validation of the sub-metric accuracy of vertical positioning of PS's in C band. IEEE Geoscience and Remote Sensing Letters 5 (3), 502–506.

Perissin, D, 2010. Atmospheric Modelling. Chapter 2. Metawave Report.

Wadge, G., Webley, P.W., James, I.N., Bingley, R., Dodson, A., Waugh, S., et al., 2002. Atmospheric models, GPS and InSAR measurements of the tropospheric water vapour field over Mount Etna. Geophysical Research Letters 29 (19), 1905 http://dx.doi.org/10.1029/2002GL015159.

Williams, S., Bock, Y., Fang, P., 1998. Integrated satellite interferometry: Troposphere noise, GPS estimates, and implications for synthetic aperture radar. Journal of Geophysical Research 103 (B11), 27051–27067.

Xu, C., Wang, H., Ge, L., et al., 2006. InSAR tropospheric delay mitigation by GPS observations: A case study in Tokyo area. Journal of Atmospheric and Solar-Terrestrial Physics 68, 629–638.

Zebker, H.A., Rosen, P.A., Hensley, S., 1997. Atmospheric effects in interferometric synthetic aperture radar surface deformation and topographic maps. Journal of Geophysical Research 102 (B4), 7547–7563.